THE JOURNAL OF BIOLOGICAL CHEMISTRY VOL. 290, NO. 20, pp. 12451–12462, May 15, 2015
Published in the U.S.A.

Dimeric c-di-GMP Is Required for Post-translational Regulation of Alginate Production in *Pseudomonas aeruginosa*[*]

Received for publication, February 11, 2015, and in revised form, March 16, 2015 Published, JBC Papers in Press, March 27, 2015, DOI 10.1074/jbc.M115.645051

John C. Whitney[‡§1,2], Gregory B. Whitfield[‡§1,3], Lindsey S. Marmont[‡§4], Patrick Yip[‡], A. Mirela Neculai[‡], Yuri D. Lobsanov[‡], Howard Robinson[¶], Dennis E. Ohman[‖], and P. Lynne Howell[‡§5]

From the [‡]Program in Molecular Structure and Function, Hospital for Sick Children, Toronto, Ontario M5G 0A4, Canada, the [§]Department of Biochemistry, University of Toronto, Toronto, Ontario M5S 1A8, Canada, the [¶]Photon Sciences Division, Brookhaven National Laboratory, Upton, New York 11973-5000, and the [‖]Department of Microbiology and Immunology, Virginia Commonwealth University Medical Center and McGuire Veterans Affairs Medical Center, Richmond, Virginia 23298-0678

Background: Alg44 regulates the production of alginate in *Pseudomonas aeruginosa* via c-di-GMP binding.
Results: The structure of the PilZ domain of Alg44 in complex with c-di-GMP reveals residues that control c-di-GMP/Alg44 stoichiometry.
Conclusion: Binding of dimeric c-di-GMP is required for alginate biosynthesis.
Significance: This is the first example of a receptor requiring a specific form of c-di-GMP for activation.

Pseudomonas aeruginosa **is an opportunistic human pathogen that secretes the exopolysaccharide alginate during infection of the respiratory tract of individuals afflicted with cystic fibrosis and chronic obstructive pulmonary disease. Among the proteins required for alginate production, Alg44 has been identified as an inner membrane protein whose bis-(3′,5′)-cyclic dimeric guanosine monophosphate (c-di-GMP) binding activity post-translationally regulates alginate secretion. In this study, we report the 1.8 Å crystal structure of the cytoplasmic region of Alg44 in complex with dimeric self-intercalated c-di-GMP and characterize its dinucleotide-binding site using mutational analysis. The structure shows that the c-di-GMP binding region of Alg44 adopts a PilZ domain fold with a dimerization mode not previously observed for this family of proteins. Calorimetric binding analysis of residues in the c-di-GMP binding site demonstrate that mutation of Arg-17 and Arg-95 alters the binding stoichiometry between c-di-GMP and Alg44 from 2:1 to 1:1. Introduction of these mutant alleles on the *P. aeruginosa* chromosome show that the residues required for binding of dimeric c-di-GMP *in vitro* are also required for efficient alginate production *in vivo*. These results suggest that the dimeric form of c-di-GMP represents the biologically active signaling molecule needed for the secretion of an important virulence factor produced by *P. aeruginosa*.**

Bis-(3′,5′)-cyclic dimeric guanosine monophosphate (c-di-GMP)[6] is a second messenger that controls a wide range of biological processes in bacteria. High levels of c-di-GMP often correlate with the activation of cellular pathways that promote the transition from a planktonic, highly motile state to a multicellular, biofilm-embedded community (1, 2). The opportunistic pathogen, *Pseudomonas aeruginosa*, is the leading cause of morbidity and mortality among cystic fibrosis patients partly due to its ability to adopt a biofilm mode of growth (3). Biofilms, of which secreted polysaccharides comprise a major constituent, protect pathogenic bacteria from the immune response of their host as well as increase their tolerance to administered antibiotics (4). *P. aeruginosa* is capable of producing at least three exopolysaccharides that have been implicated in biofilm formation: alginate and the Pel and Psl polysaccharides (5). The majority of *P. aeruginosa* isolates are non-mucoid and utilize the Pel and/or Psl polysaccharides as the primary structural component of the biofilm matrix (6, 7). However, during chronic cystic fibrosis lung infections, *P. aeruginosa* converts to a mucoid biofilm phenotype characterized by the secretion of alginate (8). In mucoid biofilms, the Pel and/or Psl polysaccharides serve as the structural scaffold of the biofilm, whereas

* This work was supported, in whole or in part, by National Institutes of Health, NIAID, Grant AI-19146 (to D. E. O.). This work was also supported by Canadian Institutes of Health Research Grant MT13337 (to P. L. H.) and Veterans Administration Medical Research Grant IO1BX000477 (to D. E. O.). Beam line X29 at the National Synchrotron Light Source is supported by the United States Department of Energy and the National Institutes of Health National Center for Research Resources.
The atomic coordinates and structure factors (codes 4RT0 and 4RT1) have been deposited in the Protein Data Bank (http://wwpdb.org/).
[1] Both authors contributed equally to this work.
[2] Supported by graduate scholarships from the Natural Sciences and Engineering Research Council of Canada (NSERC), Cystic Fibrosis Canada (CFC), the Ontario Graduate Scholarship (OGS) Program, and the Hospital for Sick Children (SickKids) Foundation Student Scholarship Program. Present address: Dept. of Microbiology, University of Washington, Seattle, WA 98195.
[3] Supported by a graduate scholarship from NSERC.
[4] Supported in part by an undergraduate summer studentship from CFC and graduate scholarships from NSERC and the OGS and SickKids Foundation Student scholarship programs.
[5] Recipient of a Canada Research Chair. To whom correspondence should be addressed: Program in Molecular Structure and Function, Peter Gilgan Centre for Research and Learning, Hospital for Sick Children, 686 Bay St., Toronto, Ontario M5G 0A4, Canada. Tel.: 416-813-5378; Fax: 416-813-5379; E-mail: howell@sickkids.ca.

[6] The abbreviations used are: c-di-GMP, bis-(3′,5′)-cyclic dimeric guanosine monophosphate; ITC, isothermal titration calorimetry; IPTG, isopropyl 1-thio-β-D-galactopyranoside; SAD, single-wavelength anomalous dispersion; r.m.s., root mean square; SUMO, small ubiquitin-like modifier.

alginate is layered on top of this foundation to serve as a protective barrier (9). The production of alginate by *P. aeruginosa* is post-translationally regulated by intracellular c-di-GMP concentrations, demonstrating a direct role for this signaling dinucleotide in facilitating biofilm-related infection in the cystic fibrosis lung (10).

c-di-GMP synthesis is carried out by GGDEF domain-containing diguanylate cyclases, whereas c-di-GMP degradation is catalyzed by either EAL or HD-GYP domains found in c-di-GMP phosphodiesterases. Generally speaking, the activities of these enzymes are modulated to either increase or decrease the intracellular concentration of c-di-GMP through signaling cascades that are activated in response to extracellular stimuli. Although there has been a fairly extensive characterization of the biosynthesis and degradation of c-di-GMP, the scale and diversity of the downstream effector proteins responsible for the phenotypic response are continually expanding. Examples of c-di-GMP receptors identified to date include a wide range of protein domains, such as the AAA σ^{54} interaction domain of FleQ from *P. aeruginosa* (11), the non-canonical receiver (REC) domain of VpsT from *Vibrio cholerae* (12) and the degenerate (non-catalytic) EAL domains of *P. aeruginosa* FimX (13) and *Pseudomonas fluorescens* LapD (14), the degenerate GGDEF domain of *P. aeruginosa* PelD (15, 16), and the inner membrane PgaC/PgaD poly-β-1,6-*N*-acetylglucosamine synthase complex from *Escherichia coli* (17). In addition to the above-mentioned domains, the most widespread c-di-GMP receptor identified to date is the PilZ domain. Originally identified through a bioinformatics approach (18), PilZ domain-containing proteins from a variety of bacterial species have been shown to interact directly with c-di-GMP (19–21). For example, *Vibrio cholerae* VCA0042, *Pseudomonas putida* PP4397, and *P. aeruginosa* PA4608 are PilZ domain-containing proteins of unknown function capable of binding c-di-GMP (21–23). Mechanistic insight into how c-di-GMP-PilZ interactions post-translationally activate exopolysaccharide production was revealed by the structural characterization of the BcsA-BcsB cellulose synthase complex in its apo- and c-di-GMP bound forms (24, 25). c-di-GMP binding to the C-terminal PilZ domain of the cellulose synthase subunit BcsA results in a conformational change that causes the glycosyltransferase domain of this enzyme to transition from an autoinhibited to an active state, allowing for the polymerization and translocation of cellulose polymers.

An outstanding question regarding many c-di-GMP receptors is the biological significance of the differing c-di-GMP/protein stoichiometries that have been observed. Of the aforementioned c-di-GMP-binding proteins, some have been shown to bind a single molecule of the dinucleotide, whereas others are able to bind a dimeric self-intercalated form of the molecule (23, 26). For example, VCA0042 binds monomeric c-di-GMP, whereas PP4397 binds dimeric c-di-GMP although both proteins share the same overall fold (23, 26). The molecular basis for the stoichiometry between c-di-GMP and its receptor has been identified in some PilZ domains; however, the phenotypic consequences of these differences have not yet been examined.

In this study, we examined the effect of modulating c-di-GMP-receptor stoichiometry on secretion of the exopolysaccharide alginate, an important virulence factor produced by *P. aeruginosa*. Among the proteins required for alginate biosynthesis and secretion, Alg44 has been identified as a PilZ-containing inner membrane protein that post-translationally regulates alginate production (10). We have determined the x-ray crystal structure of the PilZ domain of Alg44 ($Alg44^{PilZ}$) in complex with c-di-GMP and subsequently, when probing the ligand binding site *in vitro*, identified site-specific mutants that alter the binding stoichiometry between c-di-GMP and $Alg44^{PilZ}$ from 2:1 to 1:1. The effect of this altered c-di-GMP binding stoichiometry on the ability of Alg44 to activate alginate biosynthesis was subsequently examined in *P. aeruginosa*.

EXPERIMENTAL PROCEDURES

Protein Expression and Purification—The nucleotide sequence for the *alg44* gene from *P. aeruginosa* PAO1 was obtained from the *Pseudomonas* Genome Database (27) and used to design gene-specific primers. For crystallization, the region of *alg44* encoding amino acid residues 14–122 was generated by PCR amplification from genomic DNA and TA-cloned into the Champion™ pET SUMO (Invitrogen) expression vector as per the manufacturer's instructions. The L69M (for phasing) and R95A mutations were generated using the QuikChange® Lightning site-directed mutagenesis kit (Agilent Technologies). The resulting expression plasmids encode the following fusion proteins: an N-terminal His_6 tag, the *Saccharomyces cerevisiae* Smt3 protein (SUMO), a *S. cerevisiae* Ulp1 protease (SUMO protease) cleavage site, and Alg44(14–122) L69M or Alg44(14–122) L69M/R95A. For ITC experiments, the region of *alg44* encoding amino acid residues 1–122 was PCR-amplified and cloned into the pET24a (Novagen) expression vector via its NdeI and XhoI restriction sites. This expression plasmid encodes Alg44(1–122) followed by a non-cleavable C-terminal His_6 tag. The Q16L, R17A, R21A, D44A, S46A, R87A, and R95A mutants were generated using the QuikChange® Lightning site-directed mutagenesis kit (Agilent Technologies).

For structure determination, the Alg44(14–122) L69M construct was transformed into *E. coli* B834 Met^- cells (Novagen) in minimal medium supplemented with L-selenomethionine and expressed as per the protocol of Lee *et al.* (28). All other constructs were transformed into *E. coli* BL21 CodonPlus (DE3) cells (Stratagene) and grown in lysogeny broth (LB) containing 50 μg ml^{-1} kanamycin at 37 °C. Upon reaching an A_{600} of 0.6, protein expression was induced by the addition of 1.0 mM isopropyl β-D-1-thiogalactopyranoside (IPTG) at a temperature of 25 °C for 16 h. The cell cultures were subsequently harvested by centrifugation at 2392 × *g* for 20 min, flash-frozen, and stored at −20 °C until purification.

For purification, frozen cell pellets of all constructs were thawed and resuspended in 40 ml of buffer A (50 mM Tris-HCl, pH 8.0, 300 mM NaCl, 1 mM tris(2-carboxyethyl)phosphine, 1 SIGMAFAST EDTA-free protease inhibitor mixture tablet (Sigma)) per liter of cell culture. The resulting cell suspensions were lysed by homogenization using an Emulsiflex-C3 (Avestin Inc.) at a pressure of 70–100 megapascals (three passes total). The insoluble cell lysates were then removed by centrifugation at 25,000 × *g* for 45 min, and the soluble supernatants were loaded onto 5-ml Ni^{2+}-nitrilotriacetic acid columns pre-equil-

ibrated with buffer A containing 5 mM imidazole. The majority of the contaminating *E. coli* proteins were removed from each column by a wash step using 10 column volumes of buffer A containing 20 mM imidazole followed by elution of the purified Alg44 constructs using three column volumes of buffer A containing 250 mM imidazole.

The selenomethionyl-incorporated Alg44(14–122) L69M and native Alg44(14–122) L69M/R95A proteins were then dialyzed against buffer B (20 mM Tris-HCl, pH 8.0, 150 mM NaCl, 1 mM tris(2-carboxyethyl)phosphine) for 16 h, followed by digestion with the SUMO protease (1000:1 (w/w)) for 1 h at room temperature. The resulting digestions were then passed over Ni^{2+}-nitrilotriacetic acid columns pre-equilibrated in buffer A, and the flow-through containing the untagged protein was collected. Alg44(14–122) L69M and Alg44(14–122) L69M/R95A were then further purified over a HiLoad 16/60 Superdex 75 gel filtration column (GE Healthcare) pre-equilibrated in buffer B, and the eluates were stored at 4 °C until required. Alg44(1–122) and its Q16L, R17A, R21A, D44A, S46A, R87A, and R95A mutants were purified over a HiLoad 16/60 Superdex 75 gel filtration column (GE Healthcare) pre-equilibrated in buffer C (20 mM Tris-HCl, pH 8.0, 150 mM NaCl, and 5% (v/v) glycerol), and the eluates were stored at 4 °C until required.

Preparation of c-di-GMP—The enzymatic production of c-di-GMP was carried out as described by Whitney *et al.* (16). Briefly, 3.4 μM *P. aeruginosa* $WspR^{R242A}$ was incubated at 37 °C in 50 mM Tris-HCl, pH 7.5, 50 mM NaCl, 5 mM $MgCl_2$, and 1 mM GTP for 16 h. The $WspR^{R242A}$ protein was then precipitated from the mixture by heating at 88 °C for 5 min and removed by syringe filtration (0.20 μm; Sarstedt). Triethylammonium bicarbonate was then added to the mixture to a final concentration of 5 mM prior to loading onto a 3-ml Resource RPC column (GE Healthcare). c-di-GMP was then eluted from the column using a linear gradient of 0–50% (v/v) ethanol. c-di-GMP eluted as a single peak, and its identity was confirmed by MALDI-TOF mass spectrometry (SPARC BioCentre, Hospital for Sick Children). Purified c-di-GMP was then lyophilized and stored at −20 °C until required. For subsequent experiments, the solution concentration of c-di-GMP was quantified using an extinction coefficient (ϵ_{260}) of 26,000 M^{-1} cm^{-1}.

Crystallization and Structure Determination—Selenomethionyl-incorporated Alg44(14–122) L69M and native Alg44(14–122) L69M/R95A were concentrated to 10 mg ml^{-1} by spin ultrafiltration (10 kDa molecular mass cut-off, Millipore) and screened against commercially available sparse matrix crystal screens (MCSG1–4, Microlytic) in the presence of 2.5 mM c-di-GMP (without any preincubation of the proteins and ligand). Crystal trials were set up in 48-well VDX plates using the hanging drop vapor diffusion technique. Protein and crystallization solutions were mixed in a 1:1 ratio with a final drop size of 3 μl suspended over 250 μl of crystallization solution and stored at 20 °C.

Crystals of selenomethionyl-incorporated Alg44(14–122) L69M appeared in condition 16 of the MCSG3 screen (0.1 M citric acid-NaOH, pH 3.5, 25% (w/v) PEG 3350) after 4 days. These crystals were optimized through systematic variation of the precipitant concentration and buffer pH, resulting in diffraction quality crystals that were grown in 0.1 M citric acid-NaOH, pH 2.9, 24% (*w*/*v*) PEG 3350. Crystals were cryoprotected in the crystallization solution supplemented with 20% (v/v) ethylene glycol prior to flash freezing in liquid nitrogen. X-ray diffraction data were collected on beamline X29A at the National Synchrotron Light Source at Brookhaven National Laboratory. Low resolution (180 images of 2° $\Delta\varphi$ oscillation) and high resolution (360 images of 1.0° $\Delta\varphi$ oscillation) data sets were collected on an ADSC Q315r CCD detector with a 260-mm crystal-to-detector distance and an exposure time of 0.4 s/image. The data were merged, integrated, and scaled using the HKL2000 software program. A total of three (of three) selenium sites were located using HKL2MAP, and density-modified phases were calculated using SOLVE/RESOLVE. The resulting density-modified Se-SAD map was of excellent quality and allowed for automated model building with Phenix AutoBuild (29). Subsequent model adjustments were made manually in COOT (30) between iterative rounds of refinement, which was carried out with PHENIX.REFINE (31). The progress of the refinement was monitored as a function of the reduction and convergence of R_{work} and R_{free} (Table 1).

Crystals of Alg44(14–122) L69M/R95A appeared in condition 72 of the MCSG3 screen (0.1 M HEPES-NaOH, pH 7.5, 30% (*v*/*v*) PEG 400, 0.2 M NaCl) after 7 days. These crystals were directly flash-frozen from the hit condition, and x-ray diffraction data were collected on beamline X29A at the National Synchrotron Light Source. Data were processed using HKL2000, and the structure was determined using the PHENIX AutoMR wizard with the wild-type protein as a search model and refined as described above.

Limited Proteolysis—Alg44(1–122) at a concentration of 1 mg ml^{-1} was incubated with porcine trypsin (Sigma) at a ratio of 1000:1 (w/w) in the absence and presence of 1 mM c-di-GMP. Time points were taken at 0, 15, 30, 60, 120, 180, and 240 min by taking 5-μl aliquots of the reaction mixture directly added into Laemmli buffer and heating it to 95 °C for 5 min. Samples were run on SDS-PAGE using 16% polyacrylamide Tris-glycine gels and stained with Coomassie Brilliant Blue G-250. Identification of the trypsin cleavage site was done by Edman sequencing (SPARC BioCentre, The Hospital for Sick Children).

Isothermal Titration Calorimetry—Alg44(1–122), Q16L, R17A, R21A, D44A, S46A, R87A, and R95A variants and c-di-GMP were prepared in buffer C, and each solution was degassed before experimentation. ITC measurements were performed with a VP-ITC microcalorimeter (MicroCal Inc., Northampton, MA). Titrations were carried out with 500 μM c-di-GMP in the syringe and the following concentrations of the indicated Alg44(1–122) samples in the cuvette: 15 μM wild type, 40 μM Q16L, 30 μM R17A, 15 μM R21A, 15 μM D44A, 15 μM S46A, 15 μM R87A, and 40 μM R95A. Each titration experiment consisted of 25 10-μl injections with 240-s intervals between each injection. The heats of dilution for titrating c-di-GMP into buffer were subtracted from the sample data prior to analysis. The ITC data were analyzed using the Origin version 5.0 software (MicroCal Inc.) and fit using the appropriate binding model.

Strain Construction—Chromosomal point mutations were constructed using an unmarked, non-polar allelic replacement strategy (32). A fragment containing the last 150 base pairs at

the 3′ end of *alg8* and the first 450 base pairs from the 5′ end of *alg44* was amplified from *P. aeruginosa* PAO1 genomic DNA, allowing for ~200 base pairs on either side of the codons corresponding to Gln-16 and Arg-95 of Alg44. This fragment was inserted into the suicide vector pENTRPEX18Gm using Gateway destination cloning (Invitrogen), and the plasmid pENTRPEX18Gm::*alg44* was verified by sequence analysis (Center for Applied Genomics, Hospital for Sick Children). The Q16L, R17A, R21A, D44A, S46A, R87A, and R95A point mutants were generated from pENTRPEX18Gm::*alg44* using the QuikChange® Lightning site-directed mutagenesis kit (Agilent Technologies), and each plasmid was verified by sequence analysis. Allelic exchange plasmids were conjugated into *P. aeruginosa* PAO1 by biparental mating with *E. coli* SM10 (33). Single recombinant mutants were selected on LB agar containing 30 μg ml^{-1} gentamicin and 25 μg ml^{-1} Irgasan. Double recombinant mutants were selected on LB agar without NaCl containing 15% (w/v) sucrose and were confirmed by sequence analysis.

Stimulation of Alginate Production—The full-length gene corresponding to the alternate sigma factor *algU* (*algT*) was amplified from *P. aeruginosa* PAO1 genomic DNA, using primers that introduced a *P. aeruginosa*-compatible ribosome binding site (RBS), and ligated into the IPTG-inducible *P. aeruginosa* expression vector pPSV39 (34). The plasmid pPSV39::RBS-*algU* was verified by sequence analysis and was transformed into *P. aeruginosa* strains by electroporation. Alginate production was induced by plating transformants on LB agar containing 30 μg ml^{-1} gentamicin and 1 mM IPTG.

Alginate Purification—*P. aeruginosa* strains, containing pPSV39::RBS-*algU*, were streaked onto LB agar containing 30 μg ml^{-1} gentamicin and 1 mM IPTG and allowed to grow overnight. The next day, cells were scraped from the plate and resuspended in 20 ml of 0.9% NaCl, followed by centrifugation at 2000 × *g* for 30 min to separate cells from the dissolved alginate. The cell pellet was washed once with 5 ml of 0.9% NaCl, and the alginate-containing supernatants were combined. Cell pellets were dried and weighed for analysis. Alginate was precipitated from the supernatant by the addition of an equal volume of ice-cold isopropyl alcohol, followed by centrifugation (2000 × *g* for 30 min) to pellet the alginate. Alginate pellets were resuspended in 25 ml of 0.9% NaCl and precipitated again with an equal volume of ice-cold isopropyl alcohol. Alginate pellets were dried and resuspended in 1 ml of double-distilled H_2O for subsequent analysis.

Quantification of Alginate—The concentration of purified alginate was determined by the carbazole method of Knutson and Jeanes (35). Briefly, 30 μl of purified alginate was mixed with 1 ml of ice-cold borate-sulfuric acid reagent (100 mM H_3BO_3 in concentrated H_2SO_4), followed by the addition of 30 μl of carbazole reagent (0.1% (w/v) in anhydrous ethanol). The solution was heated to 55 °C for 30 min and subsequently cooled on ice. Alginate concentration was measured spectrophotometrically at 530 nm, using alginic acid from brown seaweed as a standard.

Antibody Production and Purification—Alg44(1–122) was purified as described above. Purified Alg44(1–122) was used to generate antiserum from rabbits using a 70-day standard protocol (Cedarlane Laboratories). The α-Alg44 antiserum was further purified using a method adapted from Salamitou *et al.* (36). Briefly, 300 μg of purified Alg44(1–122) was loaded onto a 14% Tris-HCl polyacrylamide gel and transferred to a polyvinylidene fluoride (PVDF) membrane. The membrane was stained with Ponceau S, and the band corresponding to Alg44(1–122) was cut out and blocked using phosphate-buffered saline (PBS), pH 7, with 0.1% Tween 20 and 5% skim milk powder for 1 h. The membrane was then incubated with α-Alg44 antiserum overnight at 4 °C, followed by 2 h at room temperature. After washing with PBS, the α-Alg44 antibodies were eluted from the membrane by the addition of 700 μl of 0.2 M glycine, pH 2.2, for 15 min, followed by 300 μl of 1 M K_2HPO_4 to neutralize the solution. Antibodies were dialyzed into PBS for 24 h, mixed 1:1 with 100% glycerol, and used at a dilution of 1:3000.

Western Immunoblots—Cells were grown in LB to mid-log phase and harvested by centrifugation. After removal of the spent media, the cell pellet was resuspended in 50 μl of 2× Laemmli buffer and boiled for 10 min. 2.5 μl of sample was loaded onto a 14% polyacrylamide Tris-glycine gel and transferred to a PVDF membrane. The membrane was blocked in 5% skim milk in Tris-buffered saline with Tween 20 (TBST) for 30 min at room temperature. The membrane was subsequently probed with purified α-Alg44 antisera at a 1:3000 dilution or with commercial α-RNA polymerase antibody (Neoclone Biotechnologies) at 1:5000 in 1% skim milk in TBST for 1 h at room temperature. Blots were washed and probed with goat α-rabbit horseradish peroxidase (HRP)-conjugated secondary antibody (Bio-Rad) and developed using Pierce ECL Plus Western blotting substrate (Thermo Scientific).

RESULTS

Alg44^{PilZ} Is Homodimeric and Binds a Dimer of c-di-GMP at Its N Terminus—Previously, PhoA fusion analysis showed that Alg44 contains an N-terminal PilZ domain, a central transmembrane domain, and a C-terminal periplasmic membrane fusion protein domain (37) (Fig. 1*A*). To examine the c-di-GMP binding properties of Alg44, studies of Alg44^{PilZ} utilized constructs that omitted the transmembrane helix and the periplasmic domain. For structural analysis, the first 13 amino acids of the N terminus and the linker region connecting the PilZ domain to the inner membrane were omitted because bioinformatics analyses suggested that these protein segments contain a significant amount of disorder (data not shown). After generation of several constructs with varying N and C termini, the boundaries of Alg44 that were amenable to crystallization were identified as residues 14–122. Alg44(14–122) does not contain any methionine residues that can be utilized for phasing; therefore, a methionine was introduced at Leu-69 by site-directed mutagenesis. Multiple mutants were made and assessed, and the L69M mutant exhibited solubility properties that were most similar to the wild-type protein. In addition, a homology model of Alg44 predicted that this residue would be on the opposite face of the protein to the c-di-GMP binding site and therefore should not interfere with nucleotide binding. Selenomethionine-incorporated Alg44(14–122) L69M crystallized readily in the presence of c-di-GMP, and the 1.8 Å struc-

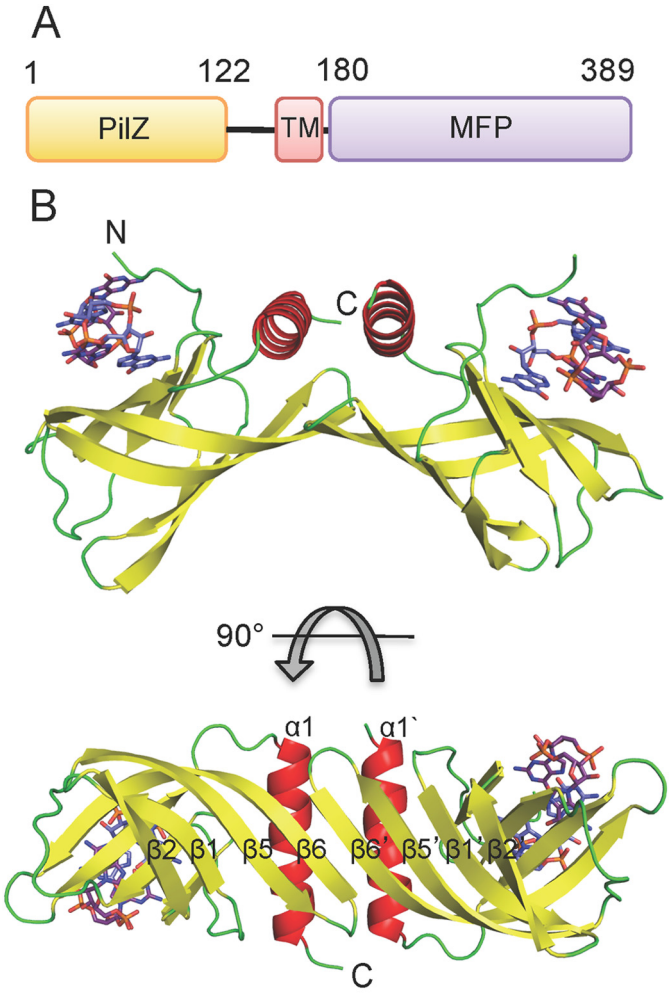

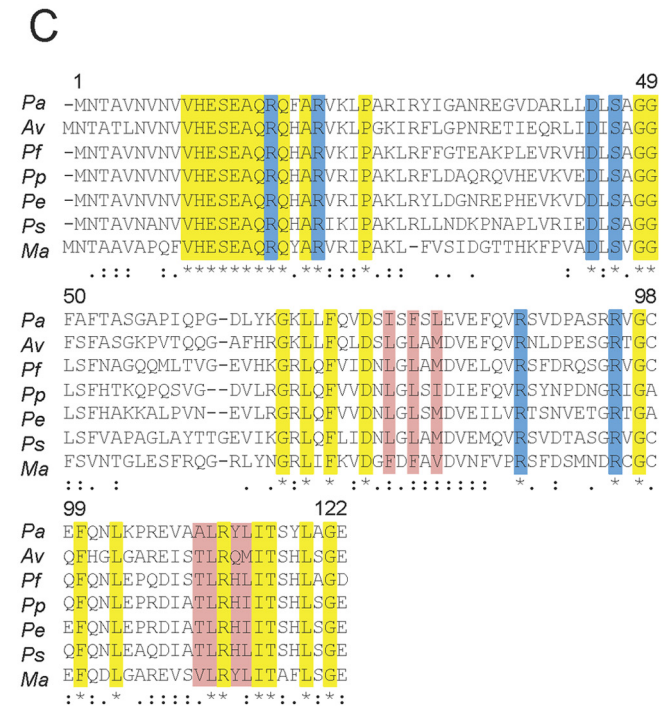

FIGURE 1. **Overall structure and conserved residues of Alg44^{PilZ}.** *A*, domain organization of full-length Alg44. *TM* and *MFP*, predicted transmembrane domain and the membrane fusion protein domain, respectively. The approximate boundaries of each domain are indicated on the diagram. *B*, structure of L69M Alg44^{PilZ} displayed as a *schematic representation* shown from two orthogonal views. The locations of the N and C termini for the monomer on the *left* are indicated with *N* and *C*, respectively. The self-intercalated c-di-GMP dimer is shown as a *stick representation* with carbon, nitrogen, oxygen, and phosphorous atoms *colored purple*, *blue*, *red*, and *orange*, respectively. *C*, multiple-sequence alignment of Alg44^{PilZ}. *Symbols below* the alignment indicate invariant (*, *highlighted yellow*), highly conserved (:), and moderately conserved (.) amino acids. Residues that comprise the c-di-GMP binding site and the homodimerization interface are *highlighted* in *blue* and *red*, respectively. *Pa*, *P. aeruginosa*; *Av*, *Azotobacter vinelandii*; *Pf*, *P. fluorescens*; *Pp*, *P. putida*; *Pe*, *Pseudomonas entomophila*; *Ps*, *Pseudomonas syringae*; *Ma*, *Marinobacter algicola*. The amino acid numbering corresponds to the *P. aeruginosa* sequence.

TABLE 1
X-ray data collection and refinement statistics

	Alg44(14–122) L69M + c-di-GMP	Alg44(14–122) L69M/R95A + c-di-GMP
Data collection		
Wavelength (Å)	0.979	1.075
Space group	$P3_121$	$P6_322$
Cell dimensions		
a, *b*, *c* (Å)	57.2, 57.2, 178.4	106.1, 106.1, 122.3
α, β, γ (degrees)	90.0, 90.0, 120.0	90.0, 90.0, 120.0
Resolution (Å)	50.0-1.80 (1.86-1.80)[a]	50.00-1.70 (1.76-1.70)
Total no. of reflections	758,769	1,745,650
Total no. of unique reflections	32,536	45,320
R_{merge} (%)[b]	6.3 (68.5)	14.7 (61.2)
$I/\sigma I$	56.7 (5.4)	36.7 (7.3)
Completeness (%)	100.0 (100.0)	100.0 (100.0)
Redundancy	23.3 (21.4)	38.5 (34.9)
Refinement		
R_{work}/R_{free} (%)[c]	18.7/21.8	16.5/20.1
No. of atoms		
Protein	2431	2604
c-di-GMP	276	138
Water	169	377
Average *B*-factors (Å^2)		
Protein	38.2	23.8
c-di-GMP	41.8	22.4
Water	42.4	34.6
r.m.s. deviations		
Bond lengths (Å)	0.009	0.010
Bond angles (degrees)	1.375	1.374
Ramachandran plot (%)[d]		
Total favored	96.5	97.7
Total allowed	99.4	100.0
Coordinate error (Å)[e]	0.20	0.15

[a] Values in parentheses correspond to the highest resolution shell.
[b] $R_{merge} = \Sigma\Sigma|I(k) - \langle I\rangle|/\Sigma I(k)$, where $I(k)$ and $\langle I\rangle$ represent the diffraction intensity values of the individual measurements and the corresponding mean values. The summation is over all unique measurements.
[c] $R_{work} = \Sigma\,||F_{obs}| - k|F_c||/|F_o|$, where F_o and F_c are the observed and calculated structure factors, respectively. R_{free} is the sum extended over a subset of reflections (5%) excluded from all stages of the refinement.
[d] As calculated using MOLPROBITY (51).
[e] Maximum likelihood-based coordinate error, as determined by PHENIX (31).

ture was determined by the single-wavelength anomalous dispersion (SAD) technique. Alg44(14–122) L69M in complex with c-di-GMP crystallized in the trigonal space group $P3_121$ with three protomers in the asymmetric unit. The density-modified SAD maps were of excellent quality and allowed for automated model building for the majority of the protein except for the N-terminal c-di-GMP binding region of Alg44(14–122) L69M as well as c-di-GMP itself, which were built manually. The final model was refined to an R_{work} and R_{free} of 18.7 and 21.8%, respectively (Table 1).

Alg44(14–122) L69M adopts a split barrel-like fold composed of six anti-parallel β-strands followed by an α-helix that sits across one end of the barrel in an orientation that is roughly

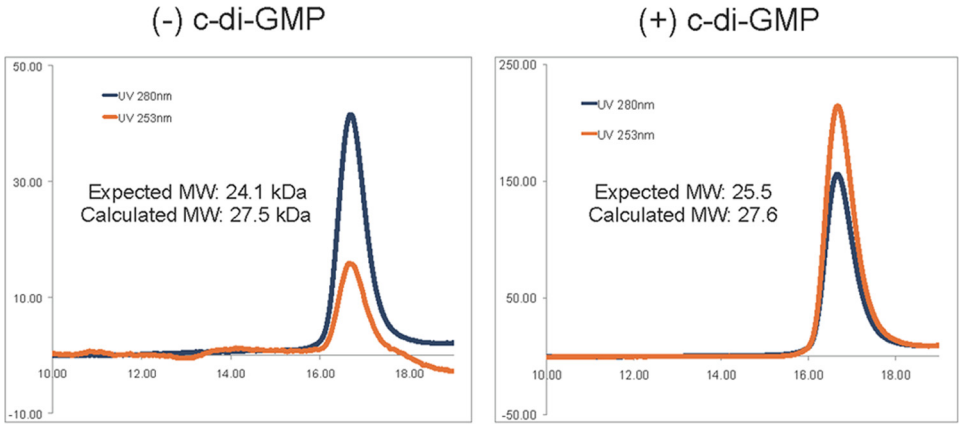

FIGURE 2. **c-di-GMP binding does not modulate the oligomeric state of Alg44^{PilZ}.** Analytical size exclusion profiles of Alg44^{PilZ} in the presence and absence of 1 mM c-di-GMP. Absorbance at 280 nm was used to monitor the elution of Alg44^{PilZ}, whereas absorbance at 253 nm (λ_{max} of c-di-GMP) was used as a qualitative indicator of c-di-GMP binding. Protein standards used to calibrate the column are indicated by *inverted triangles*; *A*, aldolase; *C*, conalbumin; *O*, ovalbumin; *R*, ribonuclease A. The molecular masses of aldolase, conalbumin, ovalbumin, and ribonuclease A are 158.0, 75.0, 43.0, and 13.7 kDa, respectively. The calculated dimeric molecular mass of Alg44^{PilZ} in the absence and presence of c-di-GMP is 27.5 and 27.6 kDa, respectively, compared with their expected molecular masses of 24.1 and 25.5 kDa.

perpendicular to the barrel axis (Fig. 1*B*). The topology of Alg44(14–122) L69M is similar to that of other PilZ domain-containing proteins that have been solved in complex with c-di-GMP, which includes *V. cholerae* VC0042 (26), *P. putida* PP4397 (23), and *P. aeruginosa* PA4608 (21). A search of the Protein Data Bank using the DALI server (38) indicates that Alg44(14–122) L69M has the highest structural similarity to *P. aeruginosa* PA4608 (Protein Data Bank code 2L74, DALI *Z*-score = 9.3, r.m.s. deviation of 2.9 Å over 100 equivalent Cα positions) and *P. putida* PP4397 (Protein Data Bank code 2GJG, DALI *Z*-score = 7.8, r.m.s. deviation of 2.5 Å over 95 equivalent Cα positions). The most notable difference between Alg44(14–122) L69M and other PilZ domains of known structure is its unique mode of homodimerization. Although VCA0042 and PP4397 are PilZ domain-containing proteins that homodimerize, the interaction interface in these proteins is largely mediated by their YcgR-N domains. In Alg44(14–122) L69M, however, homodimerization is mediated by β-sheet augmentation of the PilZ domain between the β6 strands of each split barrel monomer, resulting in a β-sheet composed of the β2-β1-β5-β6-β6′-β5′-β1′-β2′ strands (Fig. 1*B*). In addition, side chains from the β6 strand (Ile-76, Phe-78, and Leu-80) and the α1 helix (Ala-110, Leu-111, Tyr-113, and Leu-114) contribute significant buried surface area at the dimerization interface, which is predominantly hydrophobic in nature. Analysis of this interface by the PDBe PISA Web server (39) estimates a buried interface of 687 Å^2 and a Δ^iG value of −9.7 kcal/mol, suggesting that homodimer formation is energetically favorable. Moreover, the residues that make up this interface exhibit a high degree of conservation among Alg44 orthologs (Fig. 1*C*). Molecular weight analysis using analytical size exclusion chromatography indicates that Alg44(14–122) in the solution state is a dimer both in the absence and presence of c-di-GMP, suggesting that it is highly stable and that ligand binding does not modulate its oligomeric state (Fig. 2).

Examination of the c-di-GMP binding site shows that six conserved residues make polar contacts with the dimeric self-intercalated ligand. Arg-17, Arg-21, Asp-44, and Ser-46 are part of the canonical R*XXX*R and D*XSXX*G motifs that have been observed to bind c-di-GMP in other PilZ domain-containing proteins. The N_ϵ and $N_{\eta1}$ atoms of Arg-17 make hydrogen bonding interactions with the guanine N7 and O6 atoms, respectively, of the proximal c-di-GMP molecule, and its $N_{\eta1}$ atom also interacts with one of the phosphate groups of the distal c-di-GMP molecule (Fig. 3*A*). Similarly, the $N_{\eta1}$ and $N_{\eta2}$ atoms of Arg-21 hydrogen bond with the guanine N7 and O6 atoms, respectively, of the distal c-di-GMP molecule, and its $N_{\eta2}$ atom also interacts with a phosphate moiety of the proximal c-di-GMP molecule. Asp-44 makes hydrogen bonding interactions between its $O_{\delta1}$ atom and the guanine N1 and N2 atoms of the proximal c-di-GMP molecule. In addition, its $O_{\delta2}$ atom interacts with the $N_{\eta1}$ atom of Arg-95. The hydroxyl group of Ser-46 appears to be too far away from c-di-GMP (3.6 Å) to be involved in ligand binding despite its strict conservation among PilZ domains. This observation is not unique to Alg44, because the corresponding serine residues in *P. aeruginosa* PA4608 and *P. putida* PP4397 are also not within hydrogen bonding distance of c-di-GMP (4.3 and 3.7 Å, respectively). The remaining two c-di-GMP-binding residues, Arg-87 and Arg-95, are unique to Alg44 at the sequence level, and among Alg44 orthologs they are completely conserved. The N_ϵ atom of Arg-87 interacts with a phosphate group of the proximal c-di-GMP molecule, whereas the N_ϵ atom of Arg-95 forms a hydrogen bond with the ethereal oxygen of a ribose group on the distal c-di-GMP molecule. In addition to its previously stated interaction with the $O_{\delta1}$ atom of Asp-44, the $N_{\eta1}$ atom of Arg-95 also forms a hydrogen bond with the O6 atom of the proximal c-di-GMP molecule. Interestingly, the side chains of Arg-200 and Lys-164 of *P. putida* PP4397 appear to interact with c-di-GMP in the same manner as Arg-87 and Arg-95 of Alg44, despite originating from different locations in the primary sequence (Fig. 4). However, the contribution of these residues to c-di-GMP binding was not assessed in the analysis of the *P. putida* PP4397 binding site.

The amino acid residue that immediately precedes the R*XXX*R motif (referred to as "position X") has been shown to be important in other characterized PilZ domains. Alg44 contains

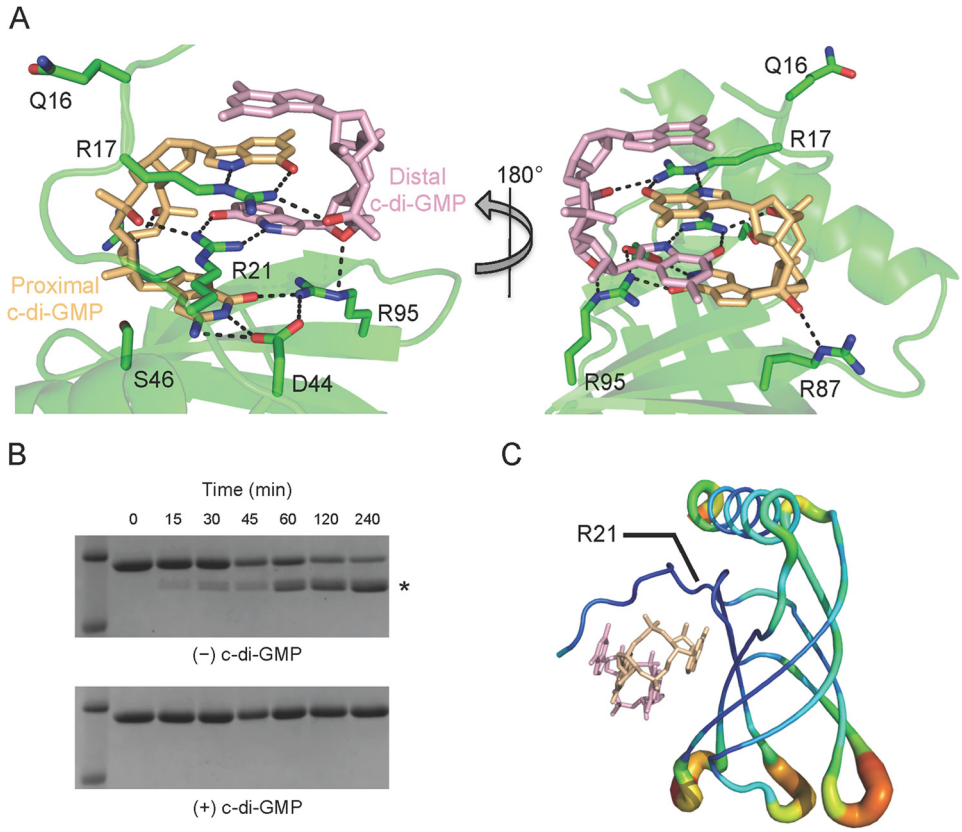

FIGURE 3. **The N terminus of Alg44^{PilZ} binds dimeric c-di-GMP.** *A*, *close-up* of the c-di-GMP binding site. Arg-17, Arg-21, Asp-44, and Ser-46 comprise the canonical R*XXX*R and D*XSXX*G motifs typically found in PilZ domains, whereas Arg-87 and Arg-95 also interact with c-di-GMP and are unique to Alg44. Gln-16 is the residue that immediately precedes the R*XXX*R motif (position X residue) that has been suggested to be important for c-di-GMP binding. Nitrogen and oxygen atoms are *colored* in *blue* and *red*, respectively. For clarity, only c-di-GMP atoms that interact with Alg44^{PilZ} residues are *colored*. Protein carbon atoms and non-Alg44^{PilZ}-interacting proximal and distal c-di-GMP atoms are *colored* in *green*, *gold*, and *light purple*, respectively. *B*, time course of trypsin proteolysis of Alg44^{PilZ} in the absence (*top*) and presence (*bottom*) of c-di-GMP. The proteolytic fragment indicated by the *asterisk* starts at Arg-21 as determined by Edman degradation (SPARC BioCentre, Hospital for Sick Children). *C*, temperature factor *putty representation* of Alg44^{PilZ}. Temperature factors are illustrated qualitatively by both the *thickness* of the backbone trace and its *color* with *blue* through to *red* representing a continuum of low to high temperature factors. The location of Arg-21 is indicated.

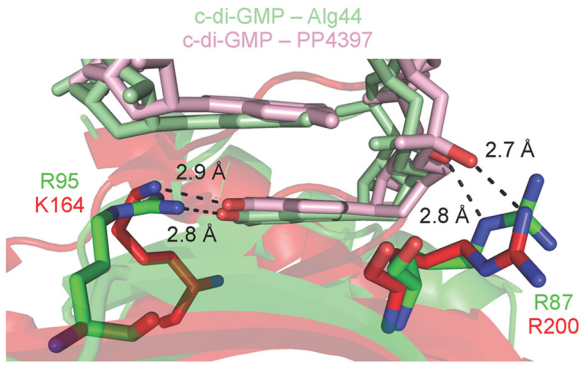

FIGURE 4. **Arg-87 and Arg-95 of Alg44^{PilZ} may be functionally equivalent to Arg-200 and Lys-164 of *P. putida* PP4397.** Alg44^{PilZ} and PP4397 are shown as *schematic representations* in *green* and *red*, respectively, with their c-di-GMP binding residues displayed as *sticks*. The c-di-GMP bound to Alg44^{PilZ} is displayed as *light green sticks* with oxygen atoms that are interacting with Alg44^{PilZ} residues *colored red*. The c-di-GMP bound to PP4397 is displayed as *pink sticks* with oxygen atoms that are interacting with Alg44^{PilZ} residues *colored red*.

a glutamine at position X, consistent with the previous observation that a hydrophilic amino acid at this position facilitates the binding of dimeric c-di-GMP (23). However, Gln-16 does not appear to make contact with c-di-GMP (Fig. 3*A*).

A solution NMR study of the PilZ domain protein PA4608 from *P. aeruginosa* demonstrated that the N-terminal c-di-GMP binding region of this protein undergoes a disorder-to-order transition upon binding the dinucleotide. The result of this rearrangement is the creation of a highly negative surface on one side of the protein that the authors propose forms the molecular basis for downstream signaling (21). Although the holo-Alg44(14–122) L69M structure does not appear to have the same charge-clustering phenomenon, we sought to determine whether the N terminus of Alg44 undergoes a similar ordering on ligand binding. Because our crystallization attempts of apo-Alg44(14–122) were unsuccessful, we used limited proteolysis to probe the dynamics of the N-terminal region. To this end, Alg44(1–122) was incubated with trypsin in the absence and presence of c-di-GMP, and its proteolytic degradation pattern was analyzed by SDS-PAGE (Fig. 3*B*). In the absence of c-di-GMP, Alg44(1–122) rapidly degraded to a lower molecular weight species, whereas in the presence of c-di-GMP, the molecular weight remained the same as that of the undigested control. Edman sequencing of this degradation product indicated that apo-Alg44(1–122) was being proteolyzed at the N-terminal side of Arg-21, confirming that the N terminus of the protein is disordered in solution but upon bind-

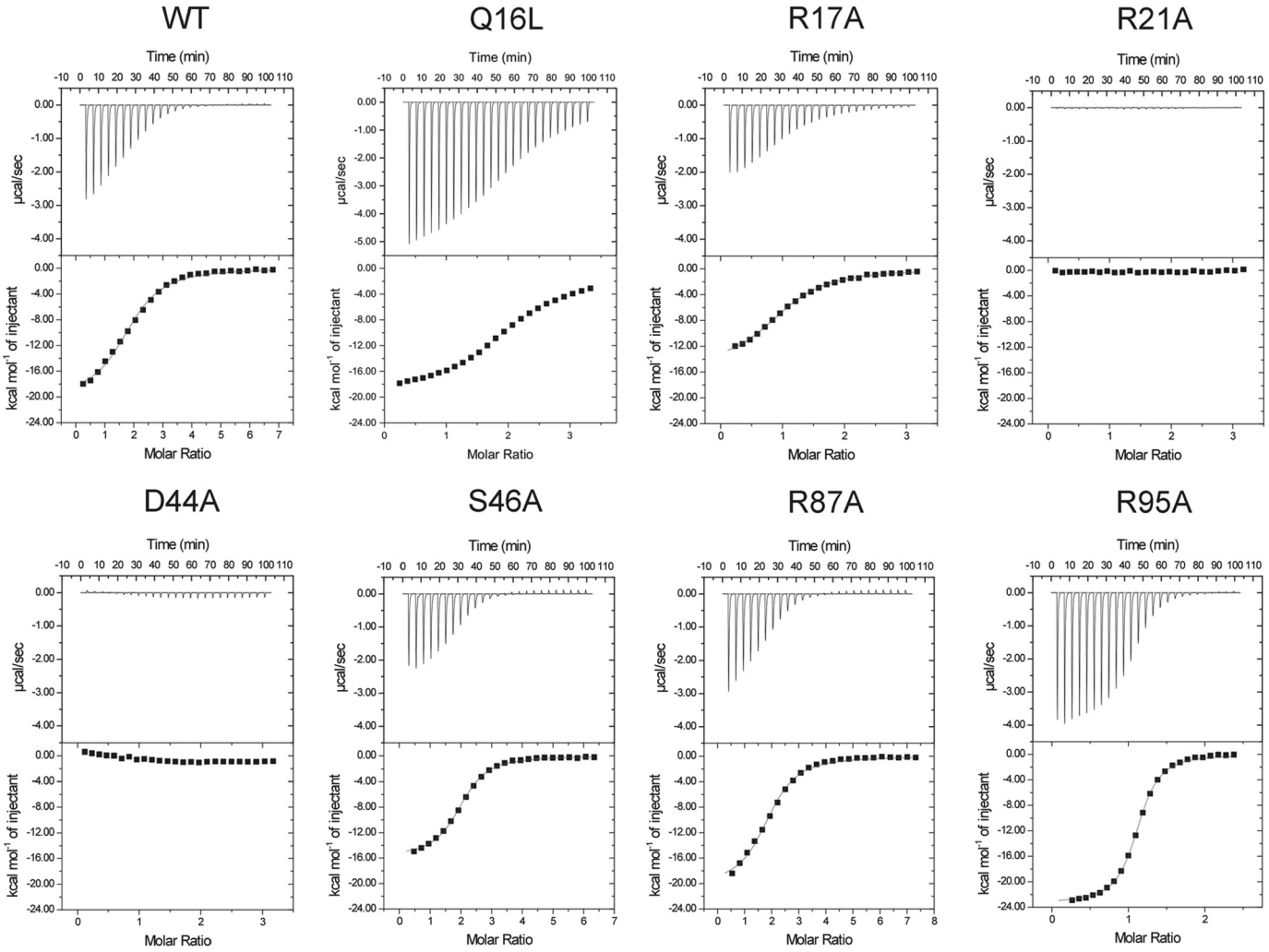

FIGURE 5. **ITC titrations of c-di-GMP with wild-type Alg44^{PilZ} and the indicated site-specific mutants.** In each experiment, the *top panel* displays the heats of injection, whereas the *bottom panel* shows the normalized integration data as a function of the molar syringe and cell concentrations. Where binding was observed, the *black line* in the *bottom panel* of each experiment represents the fit of the integrated data to an independent sites binding model. The calculated dissociation constants (K_D), binding stoichiometries, and thermodynamic parameters are listed in Table 2.

ing c-di-GMP becomes ordered and resistant to trypsin degradation (Fig. 3*C*).

Mechanism of c-di-GMP Binding—For calorimetric analysis of the c-di-GMP binding site, a construct encompassing residues 1–122 of Alg44 was generated (Alg44(1–122)). The inclusion of the first 13 amino acids of Alg44 did not change the solution properties of the protein compared with the crystallization construct (Alg44(14–122) L69M) as determined by size exclusion chromatography and circular dichroism spectroscopy (data not shown). To determine the importance of each of the previously mentioned residues in interactions with the dinucleotide, ITC analysis was performed on wild-type Alg44(1–122) as well as on R17A, R21A, D44A, S46A, R87A, and R95A site-directed mutants (Fig. 5 and Table 2). Because VCA0042 contains a leucine at position X and can only bind monomeric c-di-GMP, the corresponding Alg44 position X mutant, Q16L, was analyzed to probe binding stoichiometry. Although Gln-16 does not appear to make contact with c-di-GMP in the crystal structure of Alg44(14–122) (Fig. 3*A*), we speculated that it could still play a role in c-di-GMP interactions, given its proximity to the truncated N terminus (deletion of which was required for crystallization) as well as the limited proteolysis studies with Alg44(1–122) that suggest an N-terminal conformational change upon c-di-GMP binding.

Due to the dimeric nature of the protein, the binding of c-di-GMP to the wild type and mutant variants was fit to an independent sites binding model. For Alg44(1–122), this yielded a K_D of 3.13 ± 0.25 μM and a ligand/protein stoichiometry of 1.86 ± 0.03, suggesting that, as found in the crystal structure, two molecules of c-di-GMP bind each monomer of Alg44(1–122) (Table 2). Analysis of the Q16L, S46A, and R87A mutants revealed K_D values and stoichiometries that were similar to those of the wild-type protein, suggesting that these residues do not perturb the stoichiometry and thermodynamics of the c-di-GMP/Alg44(1–122) interaction. In contrast, the R21A and D44A mutants reduced c-di-GMP binding affinity to below the detection limit of the calorimeter, indicating that in the absence of either of these residues, c-di-GMP is unable to bind Alg44(1–122) with any appreciable affinity. The final pair of alanine mutants, R17A and R95A, were also fit to an independent sites binding model. However, unlike the WT, Q16L, S46A, and R87A samples, the calculated stoichiometry between c-di-

TABLE 2
Thermodynamic parameters of c-di-GMP binding to wild-type Alg44^{PilZ} and the indicated site-specific mutants

	Binding model	K_D	ΔH	$-T\Delta S$	n
		μM	*kcal/mol*	*kcal/mol*	
Wild type	Independent sites	3.13 ± 0.25	−20.14 ± 0.39	12.60	1.86 ± 0.03
Q16L	Independent sites	5.92 ± 0.29	−21.27 ± 0.22	14.06	2.14 ± 0.01
R17A	Independent sites	5.56 ± 0.21	−15.19 ± 0.19	8.02	1.03 ± 0.01
R21A	ND[a]				
D44A	ND				
S46A	Independent sites	1.52 ± 0.07	−15.79 ± 0.14	7.84	1.97 ± 0.01
R87A	Independent sites	2.21 ± 0.19	−20.29 ± 0.43	12.58	1.87 ± 0.03
R95A	Independent sites	0.73 ± 0.03	−23.35 ± 0.10	14.96	1.09 ± 0.01

[a] ND, not determined.

GMP and the R17A and R95A mutants was 1.03 ± 0.01:1 and 1.09 ± 0.01:1, respectively, suggesting that they are only capable of binding a monomer of c-di-GMP (Table 2).

In order to confirm the stoichiometry results obtained by ITC, structural studies were carried out on the R95A mutant. However, Alg44(14–122) L69M/R95A in the presence of c-di-GMP did not crystallize in the conditions used for the L69M protein. We hypothesized that the failure to crystallize was probably due to the loss of crystal contacts as a result of the difference in ligand/protein stoichiometry, and as a consequence, Alg44(14–122) L69M/R95A was rescreened for new crystallization conditions using commercially available sparse matrix screens. A new crystal form was obtained, which diffracted to 1.7 Å, exhibited the space group symmetry of $P6_322$, and contained three protomers in the asymmetric unit. Upon structure determination by molecular replacement using the wild-type protein as a search model, it was clear from the electron density that there was only a single c-di-GMP molecule present per Alg44(14–122) L69M/R95A monomer (Fig. 6*A*). The final model of Alg44(14–122) L69M/R95A in complex with c-di-GMP was refined to an R_{work} of 16.5% and R_{free} of 20.1%.

The overall Alg44(14–122) L69M/R95A structure closely resembles that of the L69M mutant protein with an overall Cα r.m.s. deviation of 0.8 Å (Fig. 6*B*). Inspection of the c-di-GMP binding site reveals that the position of the c-di-GMP molecule in the L69M/R95A structure is in a position very similar to that of the proximal c-di-GMP molecule in the L69M structure except that its overall position is shifted by about ~1 Å relative to the split barrel core of the PilZ domain (Fig. 6*C*). The result of this shift is that Ser-46 is now within hydrogen bonding distance (3.3 Å) of the guanine N2 atom of c-di-GMP, possibly accounting for both the increased affinity and binding enthalpy of c-di-GMP to this mutant. The bonding distances between the other residues involved in c-di-GMP binding differ no more than 0.1 Å between the L69M and L69M/R95A structure. Another notable change between the two structures is that the two guanine moieties are no longer co-planar in the R95A structure. This probably arises from the different crystal packing arrangements observed between the two structures. Although crystal packing is mediated by c-di-GMP in both crystal forms, the manner in which it does so is significantly different. In the L69M structure, hydrogen-bonding interactions between atoms from the guanine and phosphate groups of opposing c-di-GMP molecules facilitate crystal lattice formation. In contrast, in molecules A and B in the L69M/R95A structure, the opposing c-di-GMP molecules interact with one another through a π-π stacking interaction between guanine bases, which probably accounts for the deviation from co-planarity observed between the two guanine groups within each

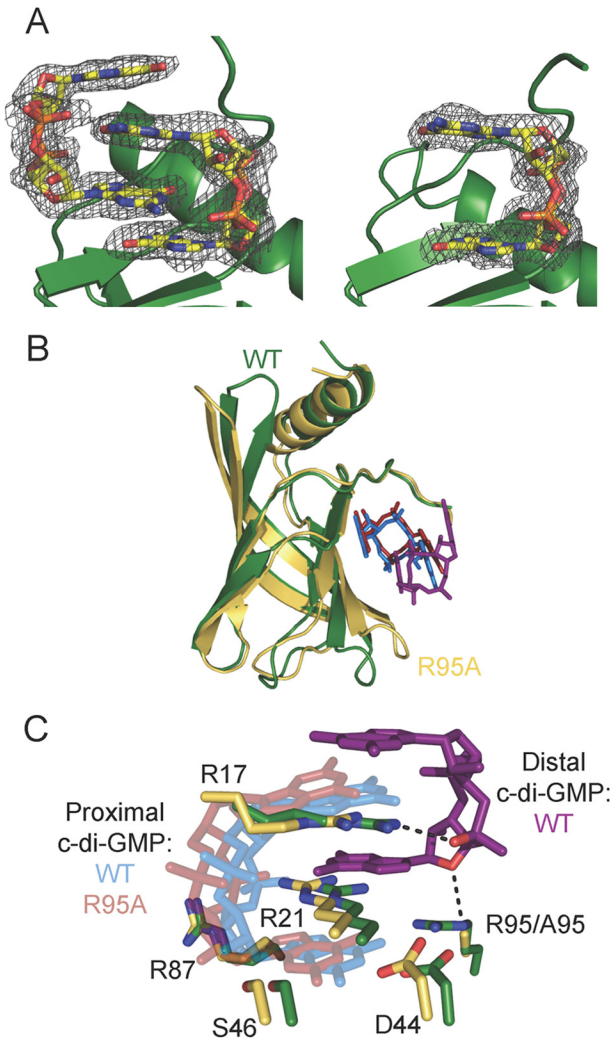

FIGURE 6. **Comparison of Alg44^{PilZ} L69M and L69M/R95A structures.** *A*, ($|F_o| - |F_c|$) electron density map, with c-di-GMP molecules omitted from the electron density calculation, contoured at 3σ and shown as a *gray mesh*, of c-di-GMP bound to L69M (*left*) and L69M/R95A (*right*) Alg44(14–122). Each protein is shown as a *schematic representation* in *green*, whereas c-di-GMP is shown as *sticks* with carbon, nitrogen, oxygen and, phosphorous atoms *colored yellow*, *blue*, *red*, and *orange*, respectively. *B*, structural overlay of the L69M Alg44^{PilZ} (*green*) and the L69M/R95A mutant (*yellow*) structures with bound c-di-GMP. *C*, structural overlay of the c-di-GMP binding residues from the L69M Alg44^{PilZ} and the L69M/R95A mutant structures. The proximal and distal c-di-GMP molecules of the L69M Alg44^{PilZ} structure are *colored light blue* and *purple*, respectively. The single bound c-di-GMP molecule of the Alg44^{PilZ} L69M/R95A mutant structure is *colored red*. The *black dashed lines* indicate polar contacts between Arg-17 and Arg-95 and the distal c-di-GMP molecule of the wild-type structure.

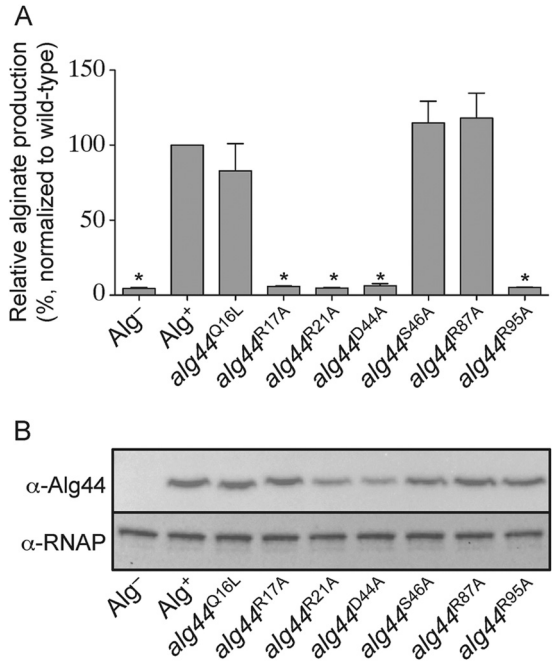

FIGURE 7. **Amino acid residues necessary for dimeric c-di-GMP binding *in vitro* are required for alginate production *in vivo*.** *A*, alginate production levels in *P. aeruginosa* PAO1 containing the pPSV39 vector control (Alg^-) or pPSV39::*algT* (Alg^+ and *alg44* site-specific mutants) grown in the presence of 1 mM IPTG. Alginate levels in strains harboring the indicated *alg44* site-specific mutant alleles were normalized to wild type (Alg^+). *Error bars*, S.D. ($n = 3$). *Asterisks*, alginate production levels that are significantly different from wild type ($p < 0.05$). *B*, Western blot analysis of the above-mentioned strains probed using α-Alg44 antibody or α-RNA polymerase (*RNAP*). RNAP was used as a loading control.

c-di-GMP molecule. The c-di-GMP moiety in molecule C of the L69M/R95A structure is not involved in crystal contacts, and its guanine groups are co-planar as per the L69M structure.

Alginate Production by P. aeruginosa Requires the Molecular Determinants for Dimeric c-di-GMP Binding—To determine whether the dimeric form of c-di-GMP is required for alginate production, the same point mutants examined by calorimetry were introduced onto the chromosome of *P. aeruginosa* PAO1 by allelic exchange. Because PAO1 does not secrete alginate under standard laboratory growth conditions, alginate production was stimulated by plasmid-born expression of the extracytoplasmic function sigma factor AlgT, which is a well characterized positive regulator of the alginate biosynthesis and export genes. In this system, induction of *algT* expression results in 97 mg of alginate per g of dry cellular mass as determined by the colorimetric carbazole assay for uronic acids (35). Importantly, PAO1 with empty vector lacking *algT* generated only 4 mg of uronic acids per g of dry cellular mass, demonstrating that the majority of uronic acids measured by this assay are due to alginate production stimulated by *algT* expression.

Next, we examined the amount of alginate produced by strains of *P. aeruginosa* bearing each of the aforementioned point mutations encoded in the native *alg44* locus (Fig. 7*A*). Consistent with the calorimetric data that demonstrated that mutation of Gln-16, Ser-46, and Arg-87 did not alter the stoichiometry or thermodynamics of c-di-GMP binding, strains expressing the Q16L, S46A, and R87A mutant variants of Alg44 exhibited levels of alginate production comparable with the wild-type background. In addition, the R21A and D44A variants, which showed no detectable c-di-GMP binding *in vitro*, were found to be unable to secrete alginate *in vivo*. Last, when the c-di-GMP stoichiometry-determining residues Arg-17 and Arg-95 were mutated to alanine on the *P. aeruginosa* chromosome, the resulting strains were also unable to produce alginate. Analysis of Alg44 levels by Western blot demonstrates that the lack of alginate production is not due to a loss of protein expression, because comparable amounts of Alg44 are expressed in all strains (Fig. 7*B*). This demonstrates the necessity for binding of dimeric c-di-GMP to Alg44 to stimulate alginate biosynthesis.

DISCUSSION

In this work, we sought to determine the number of c-di-GMP molecules required for Alg44-dependent activation of alginate production in *P. aeruginosa*. Unexpectedly, the structure of $Alg44^{PilZ}$ L69M in complex with c-di-GMP shows that this protein adopts a unique homodimeric arrangement previously unseen in the PilZ family of proteins. This observation raises the possibility that unlike the well characterized cellulose synthase complex, which requires a single PilZ domain and a single glycosyltransferase domain for polysaccharide synthesis, alginate polymerization by the putative alginate synthase complex consisting of Alg8 and Alg44 may adopt a higher order structure containing two PilZ domains and, potentially, two glycosyltransferase domains. Reconstitution and characterization of a functional alginate synthase is the focus of ongoing research in our laboratory.

Each monomer of $Alg44^{PilZ}$ L69M binds to the dimeric self-intercalated form of c-di-GMP using a constellation of six highly conserved residues. Of these residues, Arg-21 and Asp-44 are essential for binding, whereas Arg-17 and Arg-95 select for the dimeric form of c-di-GMP. Unlike other characterized c-di-GMP receptors, mutation of position X residue Gln-16 to leucine did not alter c-di-GMP binding stoichiometry and had no affect on alginate production. Crystal structures of several PilZ domain-containing proteins have shown that for some proteins, such as in VCA0042 (26), a single bound molecule of c-di-GMP is present, whereas in others, including PP4397 and PA4608 (21, 23), a self-intercalated dimer is found. In addition to observations from crystal structures, the authors of the PP4397 study were also able to alter the binding stoichiometry between c-di-GMP and PP4397 from 2:1 to 1:1 by mutating the arginine residue at position X to a leucine residue (23). Unfortunately, the biological function of each of these proteins is unknown; thus, the significance of the oligomeric state of c-di-GMP in these structures could not be ascertained. In contrast, the PilZ domain of Alg44 is a known post-translational regulator of alginate biosynthesis and secretion in *P. aeruginosa* (10, 37). Therefore, the observation that $Alg44^{PilZ}$ requires binding of dimeric c-di-GMP to stimulate alginate production demonstrates that this oligomeric state contains the molecular determinants for alginate production in *P. aeruginosa*.

A study by Pultz *et al.* showed that c-di-GMP binding affinity determines the response threshold for c-di-GMP receptors found in *Salmonella* (40). This model provides a plausible explanation for the observation that many diguanylate cyclases

appear to control only certain c-di-GMP-regulated phenotypes and not others (41). Bacteria are not known to contain any compartments that limit c-di-GMP diffusion, so it might be expected that an increase in intracellular c-di-GMP concentration would activate all c-di-GMP-responsive proteins in a given bacterium. Thus, differential ligand binding based on affinity may explain why some c-di-GMP-regulated phenotypes are observed, whereas others are not. The data presented herein add another layer of detail to this model and suggest that the oligomeric state of c-di-GMP when bound to a given receptor is probably related to its affinity for c-di-GMP. It may be that proteins only capable of binding a monomer of c-di-GMP become responsive at lower concentrations of c-di-GMP compared with those that bind the dimeric form of c-di-GMP. Consistent with this idea is the FimX protein, a c-di-GMP receptor involved in regulating type IV pili (T4P)-mediated twitching motility in *P. aeruginosa* (42). FimX binds monomeric c-di-GMP with a K_D of 100 nM, resulting in functional T4P at cellular c-di-GMP concentrations as low as 300 nM, a concentration at which exopolysaccharide synthesis is not active (13, 43, 44). However, once cellular levels of c-di-GMP reach a concentration sufficient for biofilm production (estimated to be 5–10 μM (45)), there is enough c-di-GMP present to favor its binding to exopolysaccharide-activating receptors, including Alg44, *P. aeruginosa* PelD, and *Gluconacetobacter xylinus* BcsA, which all may require the binding of two molecules of c-di-GMP for activation (16, 46). Moreover, the mechanism of product inhibition for diguanylate cyclases involves allosteric inhibition by two molecules of c-di-GMP at a conserved R*XX*D motif (termed the "I-site") that is spatially distant from their active sites (47, 48). Experimental determination of the inhibition constant (K_i) for this process is estimated to be around ~1 μM (49), which is similar to the low micromolar binding constants observed for Alg44, PelD, and BcsA (16, 46).

NMR analysis of c-di-GMP oligomerization indicates that under standard buffering conditions, the monomer/dimer equilibrium constant is around 1 mM, suggesting that at the nanomolar to micromolar concentrations found in the cell, c-di-GMP will be predominantly monomeric (50). In order to reconcile the many crystal structures of proteins bound to dimeric c-di-GMP, Gentner *et al.* (50) proposed that the dimerization process might occur on the protein with the amino acids that comprise the binding site serving as a template for dimer binding. This statement is consistent with our experimental results in that $Alg44^{PilZ}$ was only able to bind a dimer of c-di-GMP when certain amino acid residues were present. In the absence of these dimer-inducing residues, only monomeric c-di-GMP bound to Alg44. Further structural and biophysical analysis of other c-di-GMP binding domains with measurable phenotypes will allow for assessment of the generalizability of this proposed model.

REFERENCES

1. Tamayo, R., Pratt, J. T., and Camilli, A. (2007) Roles of cyclic diguanylate in the regulation of bacterial pathogenesis. *Annu. Rev. Microbiol.* **61,** 131–148
2. Mills, E., Pultz, I. S., Kulasekara, H. D., and Miller, S. I. (2011) The bacterial second messenger c-di-GMP: mechanisms of signalling. *Cell Microbiol.* **13,** 1122–1129
3. Murray, T. S., Egan, M., and Kazmierczak, B. I. (2007) *Pseudomonas aeruginosa* chronic colonization in cystic fibrosis patients. *Curr. Opin. Pediatr.* **19,** 83–88
4. Ramsey, D. M., and Wozniak, D. J. (2005) Understanding the control of *Pseudomonas aeruginosa* alginate synthesis and the prospects for management of chronic infections in cystic fibrosis. *Mol. Microbiol.* **56,** 309–322
5. Franklin, M. J., Nivens, D. E., Weadge, J. T., and Howell, P. L. (2011) Biosynthesis of the *Pseudomonas aeruginosa* extracellular polysaccharides, alginate, Pel, and Psl. *Front. Microbiol.* **2,** 167
6. Wozniak, D. J., Wyckoff, T. J. O., Starkey, M., Keyser, R., Azadi, P., O'Toole, G. A., and Parsek, M. R. (2003) Alginate is not a significant component of the extracellular polysaccharide matrix of PA14 and PAO1 *Pseudomonas aeruginosa* biofilms. *Proc. Natl. Acad. Sci. U.S.A.* **100,** 7907–7912
7. Colvin, K. M., Irie, Y., Tart, C. S., Urbano, R., Whitney, J. C., Ryder, C., Howell, P. L., Wozniak, D. J., and Parsek, M. R. (2012) The Pel and Psl polysaccharides provide *Pseudomonas aeruginosa* structural redundancy within the biofilm matrix. *Environ. Microbiol.* **14,** 1913–1928
8. Hogardt, M., and Heesemann, J. (2013) Microevolution of *Pseudomonas aeruginosa* to a chronic pathogen of the cystic fibrosis lung. *Curr. Top. Microbiol. Immunol.* **358,** 91–118
9. Yang, L., Hengzhuang, W., Wu, H., Damkiaer, S., Jochumsen, N., Song, Z., Givskov, M., Høiby, N., and Molin, S. (2012) Polysaccharides serve as scaffold of biofilms formed by mucoid *Pseudomonas aeruginosa*. *FEMS Immunol. Med. Microbiol.* **65,** 366–376
10. Merighi, M., Lee, V. T., Hyodo, M., Hayakawa, Y., and Lory, S. (2007) The second messenger bis-(3′-5′)-cyclic-GMP and its PilZ domain-containing receptor Alg44 are required for alginate biosynthesis in *Pseudomonas aeruginosa*. *Mol. Microbiol.* **65,** 876–895
11. Hickman, J. W., and Harwood, C. S. (2008) Identification of FleQ from *Pseudomonas aeruginosa* as a c-di-GMP-responsive transcription factor. *Mol. Microbiol.* **69,** 376–389
12. Krasteva, P. V., Fong, J. C. N., Shikuma, N. J., Beyhan, S., Navarro, M. V. A. S., Yildiz, F. H., and Sondermann, H. (2010) *Vibrio cholerae* VpsT regulates matrix production and motility by directly sensing cyclic di-GMP. *Science* **327,** 866–868
13. Navarro, M. V. A. S., De, N., Bae, N., Wang, Q., and Sondermann, H. (2009) Structural analysis of the GGDEF-EAL domain-containing c-di-GMP receptor FimX. *Structure* **17,** 1104–1116
14. Navarro, M. V. A. S., Newell, P. D., Krasteva, P. V., Chatterjee, D., Madden, D. R., O'Toole, G. A., and Sondermann, H. (2011) Structural basis for c-di-GMP-mediated inside-out signaling controlling periplasmic proteolysis. *PLoS Biol.* **9,** e1000588
15. Lee, V. T., Matewish, J. M., Kessler, J. L., Hyodo, M., Hayakawa, Y., and Lory, S. (2007) A cyclic-di-GMP receptor required for bacterial exopolysaccharide production. *Mol. Microbiol.* **65,** 1474–1484
16. Whitney, J. C., Colvin, K. M., Marmont, L. S., Robinson, H., Parsek, M. R., and Howell, P. L. (2012) Structure of the cytoplasmic region of PelD, a degenerate diguanylate cyclase receptor that regulates exopolysaccharide production in *Pseudomonas aeruginosa*. *J. Biol. Chem.* **287,** 23582–23593
17. Steiner, S., Lori, C., Boehm, A., and Jenal, U. (2013) Allosteric activation of exopolysaccharide synthesis through cyclic di-GMP-stimulated protein-protein interaction. *EMBO J.* **32,** 354–368
18. Amikam, D., and Galperin, M. Y. (2006) PilZ domain is part of the bacterial c-di-GMP binding protein. *Bioinformatics* **22,** 3–6
19. Whitney, J. C., and Howell, P. L. (2013) Synthase-dependent exopolysaccharide secretion in Gram-negative bacteria. *Trends Microbiol.* **21,** 63–72
20. Ryjenkov, D. A., Simm, R., Römling, U., and Gomelsky, M. (2006) The PilZ domain is a receptor for the second messenger c-di-GMP: the PilZ domain protein YcgR controls motility in enterobacteria. *J. Biol. Chem.* **281,** 30310–30314
21. Habazettl, J., Allan, M. G., Jenal, U., and Grzesiek, S. (2011) Solution structure of the PilZ domain protein PA4608 complex with cyclic di-GMP identifies charge clustering as molecular readout. *J. Biol. Chem.* **286,** 14304–14314
22. Pratt, J. T., Tamayo, R., Tischler, A. D., and Camilli, A. (2007) PilZ domain proteins bind cyclic diguanylate and regulate diverse processes in *Vibrio cholerae*. *J. Biol. Chem.* **282,** 12860–12870

23. Ko, J., Ryu, K.-S., Kim, H., Shin, J.-S., Lee, J.-O., Cheong, C., and Choi, B.-S. (2010) Structure of PP4397 reveals the molecular basis for different c-di-GMP binding modes by Pilz domain proteins. *J. Mol. Biol.* **398,** 97–110
24. Morgan, J. L. W., Strumillo, J., and Zimmer, J. (2013) Crystallographic snapshot of cellulose synthesis and membrane translocation. *Nature* **493,** 181–186
25. Morgan, J. L. W., McNamara, J. T., and Zimmer, J. (2014) Mechanism of activation of bacterial cellulose synthase by cyclic di-GMP. *Nat. Struct. Mol. Biol.* **21,** 489–496
26. Benach, J., Swaminathan, S. S., Tamayo, R., Handelman, S. K., Folta-Stogniew, E., Ramos, J. E., Forouhar, F., Neely, H., Seetharaman, J., Camilli, A., and Hunt, J. F. (2007) The structural basis of cyclic diguanylate signal transduction by PilZ domains. *EMBO J.* **26,** 5153–5166
27. Winsor, G. L., Lam, D. K. W., Fleming, L., Lo, R., Whiteside, M. D., Yu, N. Y., Hancock, R. E. W., and Brinkman, F. S. L. (2011) *Pseudomonas* Genome Database: improved comparative analysis and population genomics capability for *Pseudomonas* genomes. *Nucleic Acids Res.* **39,** D596–D600
28. Lee, J. E., Cornell, K. A., Riscoe, M. K., and Howell, P. L. (2001) Structure of *E. coli* 5′-methylthioadenosine/*S*-adenosylhomocysteine nucleosidase reveals similarity to the purine nucleoside phosphorylases. *Structure* **9,** 941–953
29. Terwilliger, T. C., Grosse-Kunstleve, R. W., Afonine, P. V., Moriarty, N. W., Zwart, P. H., Hung, L. W., Read, R. J., and Adams, P. D. (2008) Iterative model building, structure refinement and density modification with the PHENIX AutoBuild wizard. *Acta Crystallogr. D Biol. Crystallogr.* **64,** 61–69
30. Emsley, P., and Cowtan, K. (2004) Coot: model-building tools for molecular graphics. *Acta Crystallogr. D Biol. Crystallogr.* **60,** 2126–2132
31. Adams, P. D., Afonine, P. V., Bunkóczi, G., Chen, V. B., Davis, I. W., Echols, N., Headd, J. J., Hung, L. W., Kapral, G. J., Grosse-Kunstleve, R. W., McCoy, A. J., Moriarty, N. W., Oeffner, R., Read, R. J., Richardson, D. C., Richardson, J. S., Terwilliger, T. C., and Zwart, P. H. (2010) PHENIX: a comprehensive Python-based system for macromolecular structure solution. *Acta Crystallogr. D Biol. Crystallogr.* **66,** 213–221
32. Choi, K.-H., and Schweizer, H. P. (2005) An improved method for rapid generation of unmarked *Pseudomonas aeruginosa* deletion mutants. *BMC Microbiol.* **5,** 30
33. de Lorenzo, V., and Timmis, K. N. (1994) Analysis and construction of stable phenotypes in Gram-negative bacteria with Tn5- and Tn10-derived minitransposons. *Methods Enzymol.* **235,** 386–405
34. Rietsch, A., Vallet-Gely, I., Dove, S. L., and Mekalanos, J. J. (2005) ExsE, a secreted regulator of type III secretion genes in *Pseudomonas aeruginosa*. *Proc. Natl. Acad. Sci. U.S.A.* **102,** 8006–8011
35. Knutson, C. A., and Jeanes, A. (1968) A new modification of the carbazole analysis: application to heteropolysaccharides. *Anal. Biochem.* **24,** 470–481
36. Salamitou, S., Lemaire, M., Fujino, T., Ohayon, H., Gounon, P., Béguin, P., and Aubert, J. P. (1994) Subcellular localization of *Clostridium thermocellum* ORF3p, a protein carrying a receptor for the docking sequence borne by the catalytic components of the cellulosome. *J. Bacteriol.* **176,** 2828–2834
37. Oglesby, L. L., Jain, S., and Ohman, D. E. (2008) Membrane topology and roles of *Pseudomonas aeruginosa* Alg8 and Alg44 in alginate polymerization. *Microbiology* **154,** 1605–1615
38. Holm, L., and Rosenström, P. (2010) Dali server: conservation mapping in 3D. *Nucleic Acids Res.* **38,** W545–W549
39. Krissinel, E., and Henrick, K. (2007) Inference of macromolecular assemblies from crystalline state. *J. Mol. Biol.* **372,** 774–797
40. Pultz, I. S., Christen, M., Kulasekara, H. D., Kennard, A., Kulasekara, B., and Miller, S. I. (2012) The response threshold of *Salmonella* PilZ domain proteins is determined by their binding affinities for c-di-GMP. *Mol. Microbiol.* **86,** 1424–1440
41. Kulasakara, H., Lee, V., Brencic, A., Liberati, N., Urbach, J., Miyata, S., Lee, D. G., Neely, A. N., Hyodo, M., Hayakawa, Y., Ausubel, F. M., and Lory, S. (2006) Analysis of *Pseudomonas aeruginosa* diguanylate cyclases and phosphodiesterases reveals a role for bis-(3′-5′)-cyclic-GMP in virulence. *Proc. Natl. Acad. Sci. U.S.A.* **103,** 2839–2844
42. Huang, B., Whitchurch, C. B., and Mattick, J. S. (2003) FimX, a multidomain protein connecting environmental signals to twitching motility in *Pseudomonas aeruginosa*. *J. Bacteriol.* **185,** 7068–7076
43. Jain, R., Behrens, A.-J., Kaever, V., and Kazmierczak, B. I. (2012) Type IV pilus assembly in *Pseudomonas aeruginosa* over a broad range of cyclic di-GMP concentrations. *J. Bacteriol.* **194,** 4285–4294
44. Chin, K.-H., Kuo, W.-T., Yu, Y.-J., Liao, Y.-T., Yang, M.-T., and Chou, S.-H. (2012) Structural polymorphism of c-di-GMP bound to an EAL domain and in complex with a type II PilZ-domain protein. *Acta Crystallogr. D Biol. Crystallogr.* **68,** 1380–1392
45. Weinhouse, H., Sapir, S., Amikam, D., Shilo, Y., Volman, G., Ohana, P., and Benziman, M. (1997) c-di-GMP-binding protein, a new factor regulating cellulose synthesis in *Acetobacter xylinum*. *FEBS Lett.* **416,** 207–211
46. Fujiwara, T., Komoda, K., Sakurai, N., Tajima, K., Tanaka, I., and Yao, M. (2013) The c-di-GMP recognition mechanism of the PilZ domain of bacterial cellulose synthase subunit A. *Biochem. Biophys. Res. Commun.* **431,** 802–807
47. Chan, C., Paul, R., Samoray, D., Amiot, N. C., Giese, B., Jenal, U., and Schirmer, T. (2004) Structural basis of activity and allosteric control of diguanylate cyclase. *Proc. Natl. Acad. Sci. U.S.A.* **101,** 17084–17089
48. De, N., Pirruccello, M., Krasteva, P. V., Bae, N., Raghavan, R. V., and Sondermann, H. (2008) Phosphorylation-independent regulation of the diguanylate cyclase WspR. *PLoS Biol.* **6,** e67
49. Christen, B., Christen, M., Paul, R., Schmid, F., Folcher, M., Jenoe, P., Meuwly, M., and Jenal, U. (2006) Allosteric control of cyclic di-GMP signaling. *J. Biol. Chem.* **281,** 32015–32024
50. Gentner, M., Allan, M. G., Zaehringer, F., Schirmer, T., and Grzesiek, S. (2012) Oligomer formation of the bacterial second messenger c-di-GMP: reaction rates and equilibrium constants indicate a monomeric state at physiological concentrations. *J. Am. Chem. Soc.* **134,** 1019–1029
51. Chen, V. B., Arendall, W. B., 3rd, Headd, J. J., Keedy, D. A., Immormino, R. M., Kapral, G. J., Murray, L. W., Richardson, J. S., and Richardson, D. C. (2010) MolProbity: all-atom structure validation for macromolecular crystallography. *Acta Crystallogr. D Biol. Crystallogr.* **66,** 12–21